Harmful Algae 8 (2009) 478–492

Contents lists available at ScienceDirect

Harmful Algae

journal homepage: www.elsevier.com/locate/hal

Empirical models of toxigenic *Pseudo-nitzschia* blooms: Potential use as a remote detection tool in the Santa Barbara Channel

Clarissa R. Anderson [b,*], David A. Siegel [a], Raphael M. Kudela [b], Mark A. Brzezinski [c]

[a] *Institute for Computational Earth System Science, University of California, Santa Barbara, CA 93106, USA*
[b] *Ocean Sciences Department, University of California, Santa Cruz, CA 95064, USA*
[c] *Marine Science Institute and Department of Ecology, Evolution, and Marine Biology, University of California, Santa Barbara, CA 93106, USA*

ARTICLE INFO

Article history:
Received 17 March 2008
Received in revised form 6 October 2008
Accepted 7 October 2008

Keywords:
Domoic acid
Habitat models
Pseudo-nitzschia
Remote-sensing
Southern California Bight

ABSTRACT

The Santa Barbara Channel, CA is a highly productive region where wind-driven upwelling and mesoscale eddies are important processes driving phytoplankton blooms. In recent years, the spring bloom has been dominated by the neurotoxin-producing diatom, *Pseudo-nitzschia* spp. In this paper, we relate a 1.5-year time series of *Pseudo-nitzschia* spp. abundance and domoic acid concentration to physical, chemical, and biological data to better understand the mechanisms controlling local *Pseudo-nitzschia* spp. bloom dynamics. The data were used to define the ranges of environmental conditions associated with *Pseudo-nitzschia* spp. bloom development in the Santa Barbara Channel. The time series captured three large toxic events (max. particulate domoic acid concentration, pDA ~6000 ng L^{-1}; max. cellular domoic acid concentrations, cDA ~88 pg $cell^{-1}$) in the springs of 2005–2006 and summer 2005 corresponding to bloom-level *Pseudo-nitzschia* spp. abundance (>5.0 × 10^4 cells L^{-1}). In general, large increases in *Pseudo-nitzschia* spp. abundance were accompanied by increases in cDA levels, and cDA peaks preceded pDA peaks by at least one month in both the springs of 2005 and 2006. Statistical models incorporating satellite ocean color (MODIS-Aqua and SeaWiFS) and sea surface temperature (AVHRR) data were created to determine the probability that a remotely sensed phytoplankton bloom contains a significant population of toxic *Pseudo-nitzschia* spp. Models correctly estimate 98% of toxic bloom situations, with a 7–29% rate of false positive identification. Conditions most associated with high cDA levels are low sea surface temperature, high salinity, increased absorption by cDOM (412 nm), increased reflectance at 510/555 nm, and decreased particulate absorption at 510 nm. Future efforts to merge satellite and regionally downscaled forecasting products with these habitat models will help assess bloom forecasting capabilities in the central CA region and any potential connections to large-scale climate modes.

1. Introduction

Several researchers have called for long-term monitoring approaches to the study of a major toxin producer on the West Coast of North America, the diatom genus *Pseudo-nitzschia* (Trainer et al., 2000). The Southern California Bight in particular is a region where *Pseudo-nitzschia* is the dominant harmful bloom former and the only toxic group recorded in deleterious numbers for the Santa Barbara Channel (SBC) (Fryxell et al., 1997). Several *Pseudo-nitzschia* species produce the neurotoxic amino acid, domoic acid (DA), which bioconcentrates in shellfish and finfish and can result in severe, even fatal, illness for both marine mammals (Fritz et al., 1992; Scholin et al., 2000) and humans (Perl et al., 1990). DA synthesis has been linked to physiological stress in the form of silicon-, phosphate-, iron-, or copper-limitation (Pan et al., 1998; Rue and Bruland, 2001; Maldonado et al., 2002; Bates et al., 1998; Wells et al., 2005), and toxicity is not always correlated to the abundance of *Pseudo-nitzschia* spp. cells in environmental samples (Trainer et al., 2002; Marchetti et al., 2004; Anderson et al., 2006).

Correct prediction of *Pseudo-nitzschia* spp. abundance and domoic acid distributions relies on knowledge of population-specific variability over a range of local conditions. Two steps that would aid in the development of a regionally synoptic method with application to remote-sensing platforms are: (1) collection of a time series of relevant field data to identify and index environmental parameters associated with toxic bloom forcing in order to predict the probability of a toxic bloom, and (2) application of these parametric constraints to predict the probability of toxic events

* Corresponding author. Tel.: +1 805 729 0697; fax: +1 805 962 6762.
E-mail address: clrander@ucsc.edu (C.R. Anderson).

1568-9883/$ – see front matter © 2008 Elsevier B.V. All rights reserved.
doi:10.1016/j.hal.2008.10.005

from satellite-derived data for the remote assessment of new blooms and the transport of existing ones. Iglesias-Rodriguez et al. (2002) applied parametric thresholds from field data to constrain a model that uses satellite imagery to detect coccolithophorid blooms. Such a statistical approach is likely necessary for *Pseudo-nitzschia* blooms in the SBC since algorithm-based and bio-optical methods like those used for other taxa (Brown and Yoder, 1994; Subramanian and Carpenter, 1994; Stumpf et al., 2003; Westberry and Siegel, 2005; Craig et al., 2006) do not appear practical for the detection of a pennate diatom (Sathyendranath et al., 1997). With models that properly constrain the magnitudes of physical, chemical, and optical parameters associated with *Pseudo-nitzschia* blooms and toxin production, available satellite products could be utilized to remotely estimate the probability of local toxic bloom occurrence. Remote estimation would enable rapid detection and monitoring of these local toxic events when traditional shipboard measurements are not available.

The high numbers of toxic cells during bloom periods (max. 10^6 cells L^{-1}) in the SBC make HAB species a significant group for considerations of phytoplankton community structure, public health, and biogeochemical cycling. In many coastal systems, rivers are a significant source of eutrophication, but in the SBC, riverine input of nutrients appears to contribute very little to the annual nutrient budget (McPhee-Shaw et al., 2007). Time series analyses of synoptic wind forcing show the presence of upwelling-favorable winds during spring and summer in the SBC (Oey et al., 2001; Winant et al., 2003; Otero and Siegel, 2004) along with an increased probability of mesoscale eddy formation in the western portion of the Channel (Harms and Winant, 1998; Oey et al., 2001). This is a system that relies on the mixing of remineralized nutrients from deep water to support phytoplankton growth and consequently selects for spring bloom taxa capable of withstanding high upwelling shear and abrupt peaks in nutrient supply. *Pseudo-nitzschia* appears to have a high probability of blooming during or just after upwelling episodes (Trainer et al., 2000; Kudela et al., 2005). Indeed, toxic *Pseudo-nitzschia* blooms have coincided with spring upwelling in the SBC from 2002 to 2004 and have been associated with the only major stranding events reported for marine mammals in those years, indicating that such blooms may be isolated to spring months.

The results of a 1.5 year time series of *Pseudo-nitzschia* spp. abundance and domoic acid concentrations collected monthly along a channel-wide transect in the SBC are presented here and used to develop statistical models from a suite of environmental parameters. The goal of this initial model is to predict the presence or absence of bloom levels of toxic cells. Model performance is discussed in terms of the percentage of correct bloom events predicted given a set of (1) in situ and (2) remotely sensed environmental conditions.

2. Methods

Monthly cruises were conducted in the SBC aboard the R/V *Shearwater* over an 18-month period (November 2004 to June 2006) as part of the UCSB Plumes and Blooms (PnB) project to study optical, physical, biological, and chemical properties along a seven-station, cross-channel transect from Santa Cruz Island to the mainland coast (Fig. 1). The northern- and southern-most stations represent shallow, shelf sites (45 and 75 m, respectively), while the remaining sites are in waters deeper than 250 m. This total distance of approx. 40 km is sampled in a single day. Conductivity-temperature-depth (CTD) profiles were collected at each station with a Sea-Bird Electronics 911 plus CTD on a Sea-Bird Electronics SeaCat Profiler fitted with twelve 8-L Niskin bottles. Surface water samples were collected at each station for determination of

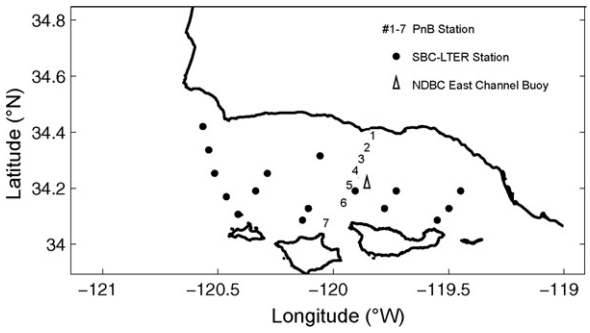

Fig. 1. At the Santa Barbara Channel (SBC) study site, seven Plumes and Blooms (PnB) stations were sampled monthly from the Santa Barbara mainland to Santa Rosa Island from November 2004 to June 2006. For validation of the *Pseudo-nitzschia* spp. abundance and toxin models, $R_{rs}(0^+, \lambda)$ values were retrieved for 16 SBC-LTER stations previously sampled during a toxigenic *Pseudo-nitzchia australis* bloom in May 2003.

chlorophyll-a concentration, dissolved inorganic nutrient concentration, phytoplankton cell abundance and domoic acid concentration. All collection procedures (excluding domoic acid samples) are in accordance with the techniques recommended by the U.S. JGOFS and SeaWiFS programs (Knap et al., 1993; Mueller and Austin, 1995).

Chlorophyll and phaeopigment analysis was performed with a Turner Designs 10AU digital fluorometer. For chlorophyll analysis, 250 mL of raw seawater were filtered through a Whatman GF/F 25 mm glass fiber filter, which was immediately frozen in liquid nitrogen and then transferred to a −70 °C freezer. Pigments for the fluorometric determination of chlorophyll and phaeopigments were extracted in 90% acetone for 24 h and fluorescence measured before and after the addition of two drops of 1.2 M HCl.

Dissolved inorganic nutrient analysis was performed by the UCSB Marine Science Institute Analytical Lab using flow injection techniques (Johnson et al., 1985) on seawater collected in 20-mL plastic scintillation vials. Detection limits for nitrate (NO_3^-), orthophosphate ($PO_4^{=}$), and silicic acid ($Si(OH)_4$) are 0.1, 0.05, and 0.2 μM, respectively.

For analysis of absorption spectra, one liter of raw seawater was filtered through a Whatman GF/F 25 mm glass fiber filter which was immediately frozen in liquid nitrogen and transferred to the laboratory. Filters were then scanned with a Shimadzu (UV-2401 UV/vis) scanning dual-beam spectrophotometer using a beta correction factor determined from the local phytoplankton population (N. Guillocheau, UCSB, personal communication). The initial absorption spectrum measures all particles on the filter (a_p). After 24–36 h of extraction in 100% methanol, the filters were re-scanned in the spectrophotometer to obtain the pigment-free, detrital absorption spectra (a_d). Absorption spectra for the phytoplankton fraction (a_{ph}) are calculated as the difference between the particulate and detrital absorption spectra. The colored dissolved, or 'gelbstoff,' fraction (a_g) is determined using a pre-rinsed, all-glass filtering rig fitted with a 47 mm, 0.2 μm membrane filter. The absorption spectrum of the filtrate is measured with the Shimadzu UV/vis spectrophotometer with a matched set of 10-cm quartz cuvettes and Millipore Q water as the reference.

Phytoplankton abundance estimates were determined from whole water samples (125-mL) collected at each station from surface Niskin bottles on a CTD rosette. Samples were preserved in 37% formalin (Bouin's solution with picric acid; Fisher Scientific) with a final concentration of 2% for phytoplankton cell counts using the Utermöhl method for the inverted microscope (Hasle, 1978). Aliquots were settled in 10- and 25-mL settling chambers for ca.

24 h. Cells over five microns in length were quantified and identified at ×320 magnification, and the abundance of *Pseudo-nitzschia* spp. was determined to the genus level.

Particulate domoic acid (pDA) analysis was performed on all surface samples collected along the PnB transect. For each sample, 500 mL of seawater were filtered through a Whatman GF/F 25-mm glass fiber filter, immediately frozen in liquid nitrogen and then transferred to a −70 °C freezer for storage. HPLC analysis of DA concentrations in the extracts was done using FMOC–Cl reagent solution to derivatize domoic acid from microalgal cells with kainic acid added as an internal standard (Pocklington et al., 1990; Wright and Quilliam, 1995). Cellular domoic acid (cDA) concentrations were derived by normalizing pDA to *Pseudo-nitzschia* spp. cell abundance and expressed in units of picograms DA cell^{-1}.

3. Results

3.1. Descriptive statistics

Over the study period November 2004 to June 2006, the abundance of *Pseudo-nitzschia* spp. in the SBC exhibited strong seasonality at all seven PnB stations with the highest cell abundance (>4.0 × 10^5 cells L^{-1}) occurring on June 2, 2005 at station 7, near Santa Cruz Island (Fig. 2a). This maximum value falls in line with the overall trend of major abundance peaks in spring months (April–June) and minor peaks in fall (September–November). Background levels of *Pseudo-nitzschia* spp. abundance in all other months have a mean of ∼1.1 × 10^4 cells L^{-1}, which is consistent with the results of an independent study showing a significant year-round presence of the *Pseudo-nitzschia* genus at a coastal site on the continental shelf in the SBC (Mengelt, 2006).

Four of the particulate and cellular DA measurements were considered extreme values (pDA: 16,000–49,000 ng L^{-1}; cDA: 208–216 pg cell^{-1}) with the potential to mask the smaller amplitudes in the time series of toxin concentration. These values far surpass those reported elsewhere from either field or laboratory studies, and so they were not included in the statistical models discussed in the next section. The time series of pDA and cDA with and without these extreme points are shown in Fig. 2b and c. In the absence of outliers, the maximum pDA (5929 ng L^{-1}) was recorded at station 6 on May 9, 2005 and the maximum cDA (88 pg cell^{-1}) on September 20, 2006 at station 2. These values are among some of the highest yet reported for the west coast of North America but are still within the range reported for blooms of *Pseudo-nitzschia* spp. from other locations (R. Kudela, personal communications Schnetzer et al., 2007; Trainer et al., 2000; Marchetti et al., 2004; Mengelt, 2006).

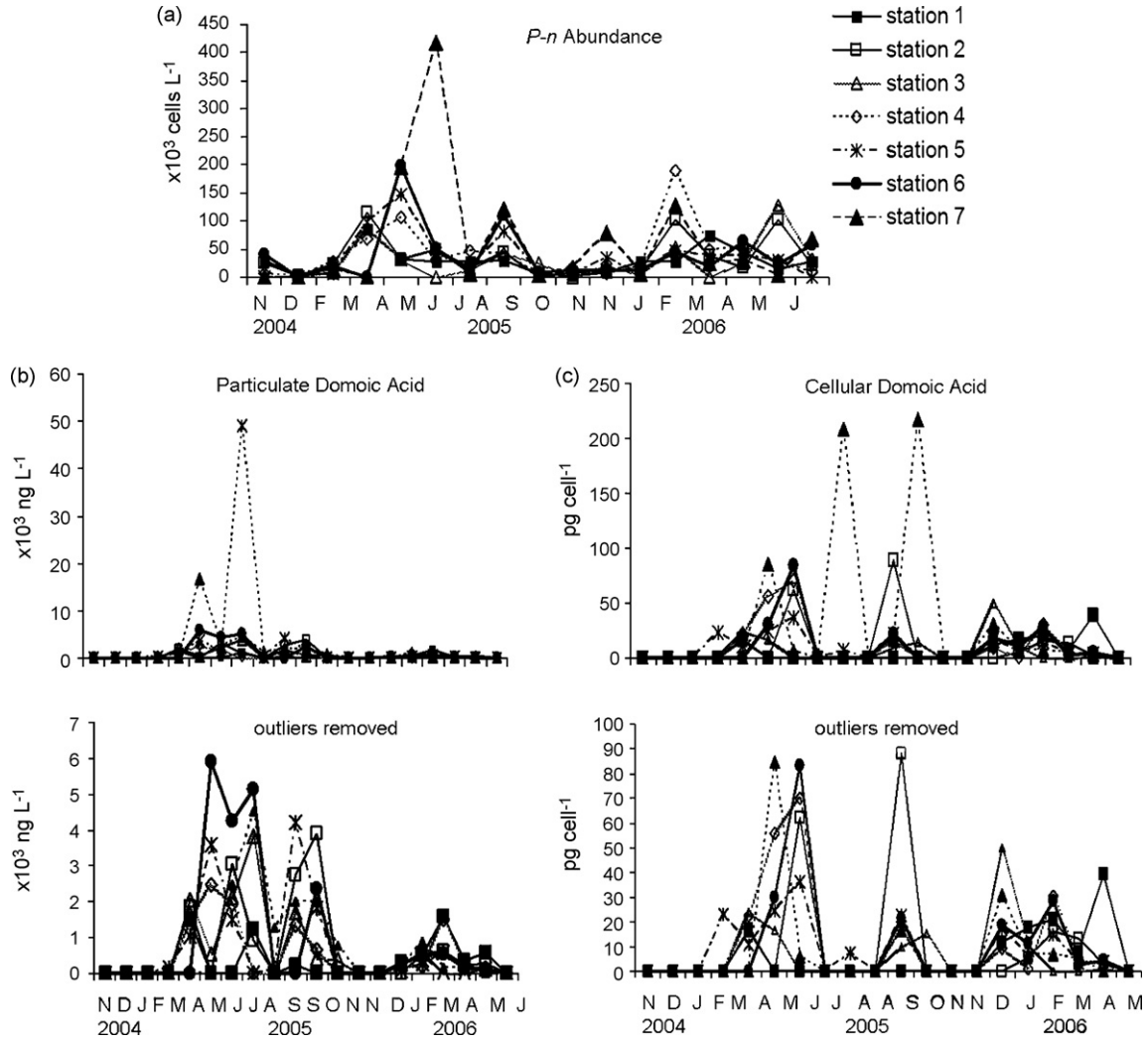

Fig. 2. Time series plots of (a) *Pseudo-nitzschia* spp. abundance, (b) particulate DA (pDA), and (c) cellular DA (cDA) sampled from November 2004 to June 2006 across the seven-station PnB transect. For pDA and cDA, the lower panels show the time series plotted without the extreme outlier points.

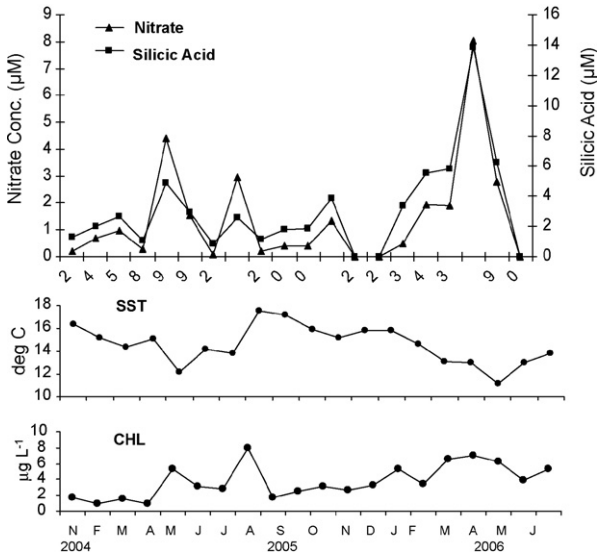

Fig. 3. Channel-wide means of nitrate (NO_3) and silicic acid ($Si(OH)_4$) concentrations, SST, and CHL over the study period. Note the missing nutrient data for the November 2005 and May–June 2006 cruises.

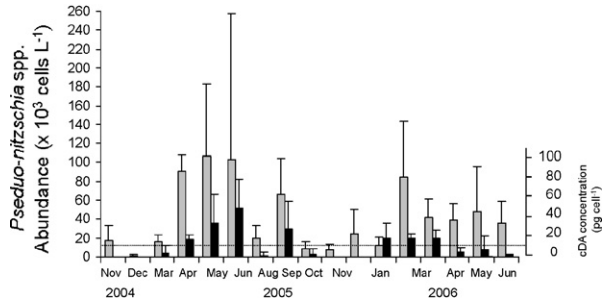

Fig. 4. Mean channel-wide *Pseudo-nitzschia* spp. abundance ($\times 10^3$ cells L^{-1}) and cDA (pg $cell^{-1}$) for each cruise; the dashed line demarcates the background mean *Pseudo-nitzschia* abundance of $\sim 1.0 \times 10^4$ cells L^{-1}.

As with cell abundance, measures of toxin concentration follow a seasonal cycle with peaks in spring and fall months, inversely related to the time series of mean sea surface temperature (SST) and directly related to time series of NO_3^-, $Si(OH)_4$, and chlorophyll (CHL) concentrations (Fig. 3). SST is significantly and negatively correlated to cell abundance and cDA level (Table 1), which points to a general association between low SST and toxic events (Figs. 2 and 3). This is consistent with the predominance of toxic bloom events occurring in the spring upwelling season, which is further supported by the significant positive correlation between pDA and sea surface salinity (SSS; Table 1). The magnitude of the spring toxic event in 2005 was significantly greater than that recorded for 2006 in terms of mean *Pseudo-nitzschia* spp. abundance, pDA, and cDA levels. However, this difference is not reflected in mean CHL biomass and is actually reversed in the nutrient field, with an obvious extreme in concentrations for March 2006 (Fig. 3). Concentrations of CHL are significantly but fairly weakly correlated to both *Pseudo-nitzschia* spp. abundance ($r = 0.34$) and pDA concentration ($r = 0.18$), indicating that the seasonal rise and fall of these parameters is not necessarily tied to the absolute magnitude of phytoplankton biomass (Table 1). It is somewhat surprising that none of the toxic bloom parameters correlate significantly with nutrient concentrations or nutrient ratios (Table 1), contrary to previous laboratory and field reports of associations between macronutrient availability and both *Pseudo-nitzschia* cell abundance and DA levels (Pan et al., 1996, 1998; Kudela et al., 2004a,b; Marchetti et al., 2004; Anderson et al., 2006).

The relationship between the frequency of toxic events and increases in abundance of *Pseudo-nitzschia* spp. is of particular relevance for the detection and prediction of harmful blooms. Out of the 77 cDA measurements in our times series (excluding the two outlier points) where *Pseudo-nitzschia* spp. abundance exceeded the mean of $\sim 1 \times 10^4$ cells L^{-1}, ~66% were above the limit of detection and ~64% were above the maximum cDA level (~2 pg $cell^{-1}$) measured during a known toxic event in the SBC (Anderson et al., 2006). Conversely, only four of the 52 cDA measurements which exceeded 2 pg $cell^{-1}$ were found to contain *Pseudo-nitzschia* cell abundances below the background mean abundance.

The mean relationship between the abundance of potentially toxic cells and cDA across all stations for each cruise is shown in Fig. 4. It is evident from this plot that the majority of bloom scenarios are accompanied by elevated cDA levels, with notable exceptions in November 2004 and 2005 when abundances just exceeding the mean were not comprised of toxic cells. In general, high *Pseudo-nitzschia* spp. abundance is accompanied by the presence of domoic acid, though more weakly related in terms of absolute magnitude. For example, a sample from station 4 on 3 March 2006 contained $\sim 1.9 \times 10^5$ cells L^{-1} but only ~1 pg DA $cell^{-1}$, while the sample containing the maximum cDA of 88 pg $cell^{-1}$ was paired with only a moderate cell count of $\sim 4.4 \times 10^4$ cells L^{-1}. Indeed, the linear regression relationship between *Pseudo-nitzschia* spp. abundance and cDA before and after the removal of outliers (Fig. 5) is rather poor (from $r^2 = 0.004$ to $r^2 = 0.12$) and only slightly improved for particulate concentrations ($r^2 = 0.28$ to $r^2 = 0.29$). A stronger relationship exists for the particulate and cellular concentrations of DA ($r^2 = 0.56$; Fig. 5), indicating that the cellular pool is more driven by pDA concentrations than cell abundance. In other words, there does not appear to be a straightforward relationship between the abundance of cells capable of producing toxin and the amount of

Table 1
Correlation coefficients (r) for select physical and chemical parameters and the abundance of *Pseudo-nitzschia* spp. (*P-n* abundance), pDA concentration, and cDA concentration (outliers removed). Bold values indicate $p < 0.05$ with DF ~ 100.

	P-n abundance	pDA	cDA	SST	SSS	CHL	NO_3	PO_4	$Si(OH)_4$	Si:N	Si:P
P-n abundance	****	**0.53**	0.07	**−0.34**	−0.15	**0.34**	0.04	0.03	0.01	−0.06	−0.07
pDA		****	**0.42**	−0.16	**0.14**	**0.18**	0.03	−0.06	−0.08	−0.08	−0.12
cDA			****	**−0.27**	0.17	0.14	−0.03	−0.06	−0.05	−0.01	−0.12
SST				****	**−0.18**	**−0.55**	**−0.62**	**−0.63**	**−0.63**	**0.38**	−0.12
SSS					****	−0.14	**0.44**	**0.32**	**0.41**	−0.11	**0.23**
CHL						****	**0.38**	**0.38**	**0.44**	**0.22**	**−0.25**
NO_3							****	**0.95**	**0.93**	0.09	−0.16
PO_4								****	**0.92**	−0.19	0.01
$Si(OH)_4$									****	−0.11	**−0.34**
Si:N										****	**0.26**
Si:P											****

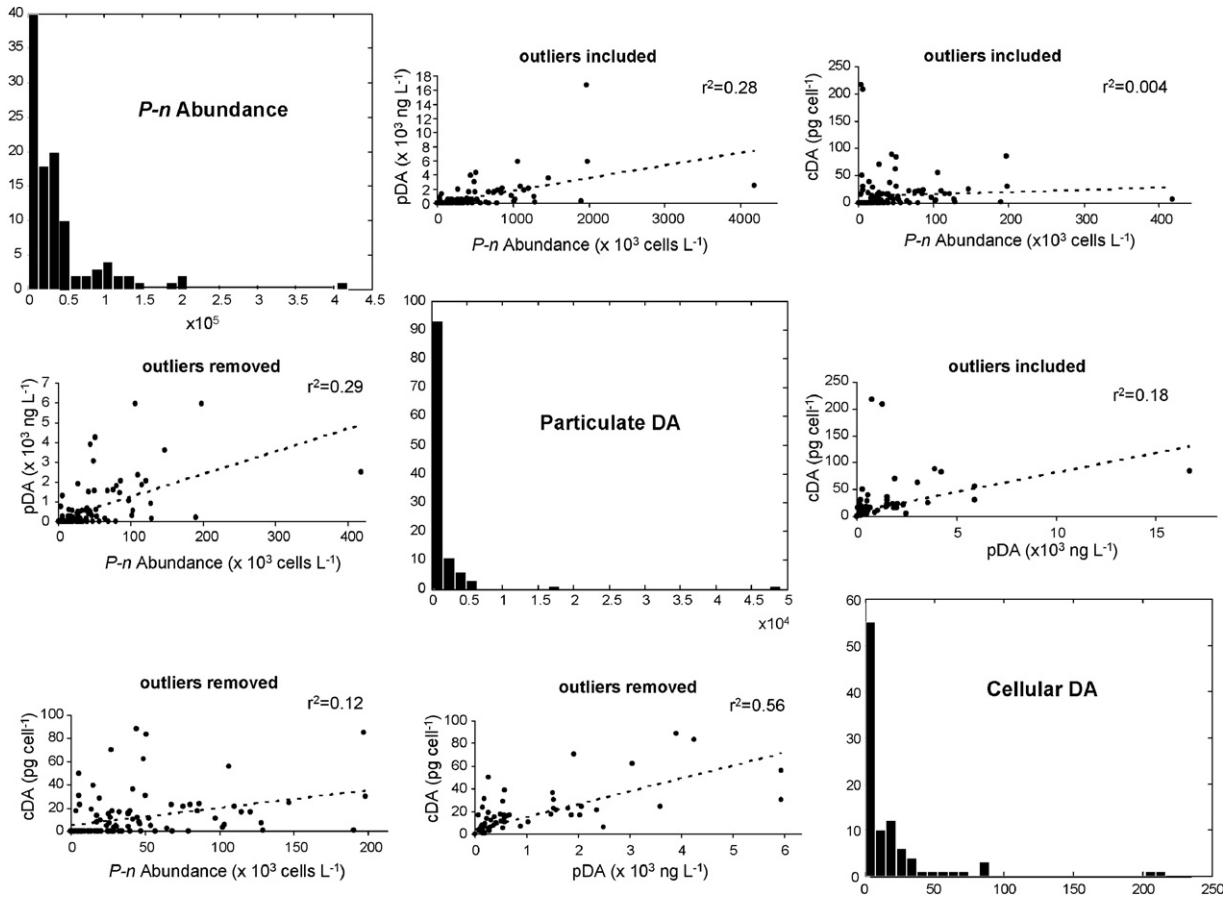

Fig. 5. A pairs plot of the response variables: *Pseudo-nitzschia* (*P-n*) abundance, particulate domoic acid concentration (pDA), and cellular domoic acid concentration (cDA). The un-transformed distributions for each parameter are highly skewed and, for pDA and cDA, clearly contain outliers (see text). The weak relationships (r^2 values) between cell abundance and toxin concentration underscore the need for predictive models of domoic acid presence in addition to *P-n* abundance.

DA present which implies that processes regulating these two parameters differ. In order to predict the occurrence of toxigenic blooms, it is thus necessary to produce separate models of *Pseudo-nitzschia* spp. abundance and DA concentration, which in combination will generate predictions of toxic events, not simply bloom events.

3.2. Predictive models of Pseudo-nitzschia abundance and DA concentration

3.2.1. Transformations and thresholds

A number of transformations were necessary to normalize the key response variables used in model development: *Pseudo-nitzschia* spp. cell abundance (hereafter referred to as *P-n* abundance), pDA, and cDA. Due to their highly skewed distributions (Fig. 5), the transformation $\log_{10}(1 + X)$ was used with the constant 1 added to avoid negative results in cases when the untransformed variable was zero. Nutrient parameters were also log-transformed due to the highly non-linear relationship between nutrient concentrations, nutrient ratios, and the three response variables (Blum et al., 2006). All transformed and untransformed variables (Table 2) were included as potential predictors in model development.

Histograms of log-transformed pDA and cDA concentrations (Fig. 6b and c) underscore that 39% and 42% of samples, respectively, were below detection levels and indicate times of low or no toxin production by *Pseudo-nitzschia* spp. in the SBC. As a

Table 2
Legend of predictor and response (in bold) variables used in hindcastor model development.

Variable	Abbreviation	Units
Station	STN	
Day of year	DOY	
Sea surface temperature	SST	°C
Sea Surface temperature-5 day mean	SST-5	°C
Sea surface salinity	SSS	psu
Chlorophyll-a	CHL	ng L^{-1}
Nitrate	NO_3	nM
Phosphate	PO_4	nM
Silicic acid	$Si(OH)_4$	nM
Remote-sensing reflectance [412–665 nm]	$R_{rs}(0^+, \lambda)$	sr^{-1}
Particulate absorption [412–665 nm]	$a_p(\lambda)$	m^{-1}
CDOM absorption [412–665 nm]	$a_g(\lambda)$	m^{-1}
Detrital absorption [412–665 nm]	$a_d(\lambda)$	m^{-1}
Silicic acid:nitrate	Si:N	
$\log_{10}$(Silicic acid:nitrate)	log(Si:N)	
Silicic acid:phosphate	Si:P	
$\log_{10}$(Silicic acid:phosphate)	log(Si:P)	
Pseudo-nitzschia spp. abundance	*P-n* abundance	cells L^{-1}
$\log_{10}$(Pseudo-nitzschia abundance)	$\log(P - N + 1)$	
Particulate domoic acid	pDA	ng L^{-1}
$\log_{10}$(Particulate domoic acid)	log(pDA + 1)	
Cellular domoic acid	cDA	pg $cell^{-1}$
$\log_{10}$(Cellular domoic acid)	log(cDA + 1)	

result, there is a distinct bi-modal distribution in both parameters, and the outliers are clearly separate from the bulk of the non-zero observations which approximate a normal distribution (Fig. 6b and c). This is made clear by the parameterized normal density curves overlaid on the histograms for cDA and pDA (Fig. 6). In contrast, there was only one water sample in which cells of *Pseudo-nitzschia* spp. were not observed (Fig. 4a), and the remaining transformed values of cell abundance approximate a log-normal distribution (Campbell, 1995).

Due to the bi-modal nature of toxin distribution (Fig. 6), the criteria for evaluating model performance were defined in terms of a cost function that distinguishes between the presence or absence of domoic acid rather than the prediction of actual concentration. The threshold for determining presence is then defined as the minimum, non-zero value observed for pDA (64 ng L^{-1}) and cDA (1.1 pg $cell^{-1}$) in the log-transformed histogram (Fig. 6). Similarly, a "bloom" threshold of 5.0×10^4 cells L^{-1} was defined for *P-n* abundance to reflect large departures in cell abundance from the mean of $\sim 1 \times 10^4$ cells L^{-1}. The cost function is cast in terms of these thresholds for cell abundance, pDA, and cDA such that model predictions can be divided into correct (#correct blooms or non-blooms predicted/#blooms or non-blooms observed) and incorrect estimates (#incorrect blooms or non-blooms/#blooms or non-blooms observed) (e.g. Brown and Yoder, 1994; Westberry and Siegel, 2005). Clearly, the placement of a given threshold in large part determines how the performance of a model is evaluated. The thresholds chosen here are based on an empirical assessment of local ranges in each parameter and are meant to constrain model predictions to scenarios which could signal the initiation of a toxic bloom in the SBC.

3.2.2. Development of linear models

It is important to differentiate between the utility of the full models in describing possible drivers of toxic *Pseudo-nitzschia* spp. blooms and the additional goal of producing models that would allow for the remote detection of the presence of toxic blooms from satellite data. For each of the three response variables discussed above, two types of model were created: (1) a full model which tests the inclusion of all measured parameters, and (2) a remote-sensing model limited to only those parameters that can be accurately estimated from satellite data. In some cases, these remote-sensing models were empirically derived using a stepwise process for selecting a best-fit model whereby only the most predictive, remote-sensing components were chosen at each step. Alternatively, the remote-sensing model was a minor manipulation of the best full models (by substitution of a maximum of three parameters with remote-sensing analogues) only in cases when this was shown to result in better model performance than the stepwise process.

Linear hindcasting is an application of linear regression technique to predictive modeling which enables the ready evaluation of a predictor and its error while describing how a given variable is related to the entire dataset (Davis, 1978; Siegel and Dickey, 1986). This method was used to statistically relate the cell abundance and toxin concentration data to the many environmental parameters measured concurrently. The three log-transformed response variables (R_i) were estimated using linear hindcasting to optimize the number of M predictor variables (P_i) in the linear model (hindcastor):

$$R_i = \sum_{i=1}^{M} \beta_i P_i + \varepsilon_i \tag{2}$$

where β_i is the parameter coefficient to be optimized by minimizing the mean square difference between the sampled and predicted data, or the residual error (ε_i). The mean squared error (e_o^2) is the expected value of the squared residuals and represents the difference between the true value of the observations and the response predicted by the model. In the context of predictability, the square root of the mean squared error (e_o) is referred to as the hindcast error. The predictive skill (S_H) of a hindcastor is evaluated using the sample variance (s^2) of the predictor variable such that:

$$S_H = \left[\frac{s^2 - e_o^2}{s^2}\right] \tag{3}$$

This hindcast skill is approximately equivalent to the r^2 value for a linear regression model and is defined as the proportion of the variance explained by a linear hindcastor. Skill values range from 0 to 1 where an $S_H = 1$ represents perfect skill (Siegel and Dickey, 1986).

The presence of chance statistical relationships between variables where no true connection exists is a problem that contributes to increases in artificial predictability as the number of predictor variables, M, is increased in the hindcastor model (2). As derived through Monte Carlo simulation by Davis (1976), the expected value of artificial skill (S_A) can be estimated from the number of inputs, M, and the effective degrees of freedom, N^*, according to the formula

$$S_A \approx \frac{M}{N^*} \tag{4}$$

The N^* value is further estimated from $N^* = N/\sigma_d$, where N is the number of data points in the record normalized by σ_d, a measure of the spatial decorrelation length. This value is the estimated integral of the spatial autocorrelation function for each response variable from zero lag to that of the first zero crossing (e.g. Siegel and Dickey, 1986). The true predictive skill (S_T) is thus defined as

$$S_T = S_H - S_A \tag{5}$$

and is the proportion of the variance explained by the linear hindcastor after accounting for artificial predictability (Siegel and Dickey, 1986; Emery and Thomson, 1997).

In order to select predictor variables which contribute the most to the estimation skill while still limiting the number of inputs M and therefore S_A, the hindcastors were developed using a stepwise approach. With each increase in the number of predictor variables M_i ($i = 1, 2, 3, \ldots$), that variable which resulted in the greatest skill, S_T, was retained and applied to each successive hindcastor model until a point was reached where, beyond M inputs, $S_T(M) > S_T(M+1)$, and there was no longer an increase in predictability. Using this approach, true skill was maximized while minimizing the number of potentially autocorrelated variables in the model that would artificially increase the hindcast skill. Each predictor variable in the final model can be weighted in terms of its order in the stepwise selection process, such that the successive placement of predictors reflects the hierarchy of explanatory power of each predictor in the hindcastor model.

Ultimately, an array of 37 physical, chemical, and optical parameters (Table 2) were selected as the most relevant inputs for model development in the prediction of the transformed cell abundance and toxin concentration variables, with no model exceeding 5 inputs before the true skill was maximized. Average SST for the 5 days preceding each PnB cruise was also included as a potential predictor in the models and was computed using a boxcar moving-average window to smooth hourly SST measurements from National Data Buoy Center (NDBC) east buoy 46053.

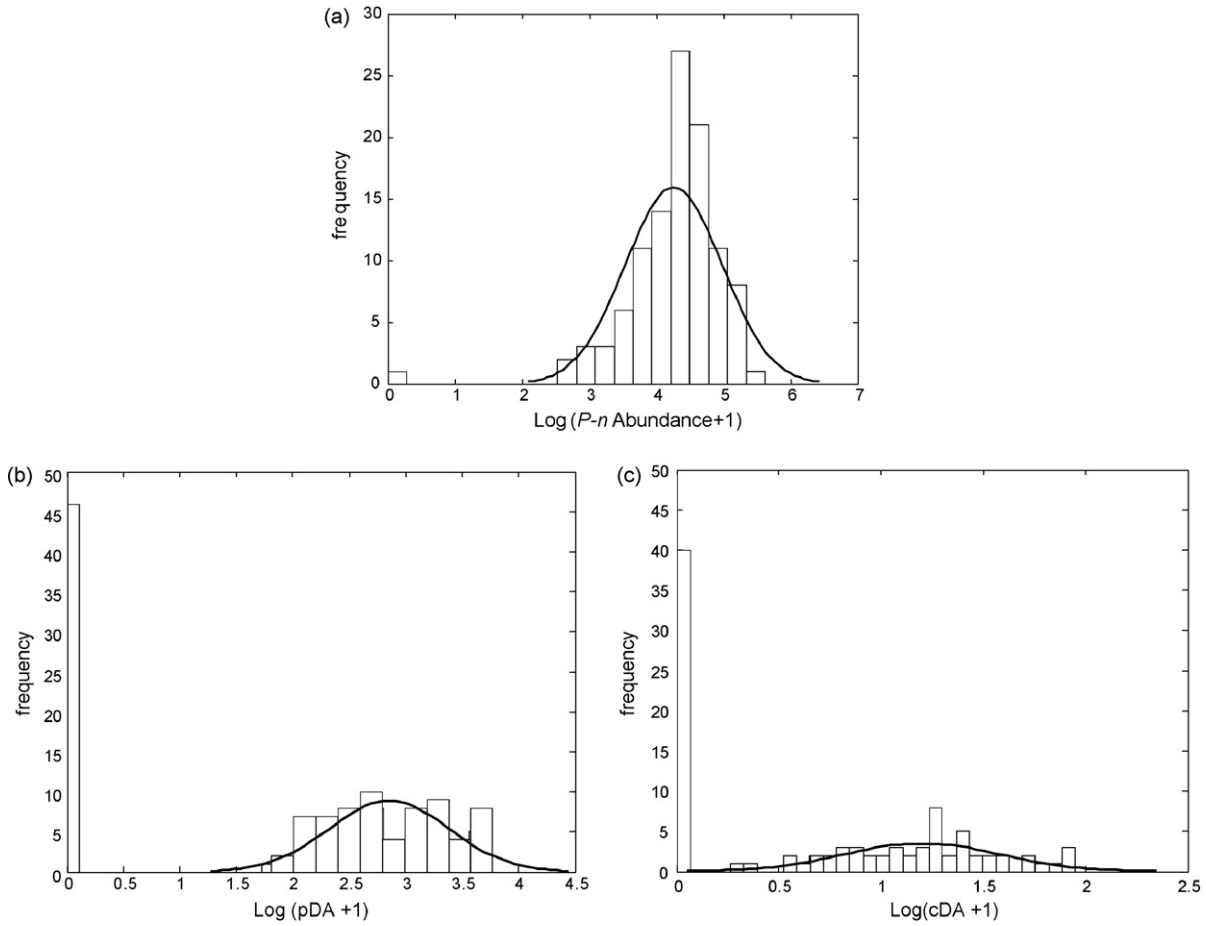

Fig. 6. Histograms of the lognormal response variables: (a) *P-n* abundance, (b) pDA, and (c) cDA (outliers removed from pDA and cDA distributions) overlaid with the approximated normal density distribution.

3.2.3. Full models

The best-fit full model for *P-n* abundance ($S_T = 0.75$, $N = 75$) is shown in Fig. 7. With the bloom threshold defined at 5.0×10^4 cells L^{-1} (~4.7 on the log-transformed scale), the model correctly predicts ~75% of bloom observations and ~93% of non-bloom observations, with ~7% incorrect non-bloom estimates or false positives (upper left quartile) and 25% false negatives. The five most predictive parameters (Table 3) for transformed *P-n* abundance were R_{rs} (412/555), ln(Si:N), R_{rs} (555), a_p(490), and R_{rs} (510/555). The negative relationship with R_{rs} (412/555) suggests increased absorption by colored dissolved organic matter (cDOM) and/or UV-absorbing accessory pigments such as those found in some red-tide dinoflagellates (Kahru and Mitchell, 1998). This could simply be due to the presence of cDOM as a by-product of terrestrial run-off and/or phytoplankton blooms *or* could signal a more interesting association between UV-absorption and *Pseudo-nitzschia* spp. blooms. Reflectance at 555 nm has been shown to be generally indicative of suspended sediment concentration (Toole and Siegel, 2001; Otero and Siegel, 2004), and R_{rs} (510/555) is used in ocean color chlorophyll algorithms (O'Reilly et al., 1998), here indicative of the presence of high chlorophyll biomass. Despite the lack of a significant correlation between the individual *Pseudo-nitzschia* abundance and nutrient parameters discussed previously (Table 1), negative log(Si:N) values explain a significant amount of the variance in *P-n* abundance according to the hindcastor model. Conversely, the significant individual correlations between *P-n* abundance and both SST and CHL established earlier (Table 1) do not prove important in explaining the overall variance of *P-n* abundance in the full model.

The true skill of the best full model for log-transformed pDA concentrations was maximized ($S_T = 0.58$, $N = 80$) at four predictor variables, which were R_{rs} (510/555), Si:P, SST, and SSS (Table 2, Fig. 7). The next most significant variable ($M = 5$) in the stepwise regression was log(Si:P) which only slightly increased the true skill and did not improve the overall performance of the hindcastor. Due to its obvious covariance with Si:P, it was excluded from the most parsimonious model. At a critical threshold value of 64 ng DA L^{-1} (~1.8 on the log-transformed scale), the best model correctly predicts ~83% of bloom and ~91% of non-bloom observations, or ~9% false positive predictions. The R_{rs} (510/555) component is again indicative of the strong negative relationship between this waveband ratio and bloom episodes. As the second most significant component in the model, the negative relationship between Si:P and pDA values suggests that either reduced $Si(OH)_4$ or increased $PO_4^{\equiv}$ values are associated with toxin production. However, given the individual negative correlations between these two macronutrients and pDA (Table 1), it is probable that the correlations are related to Si-limitation. This would seem to contradict the significant negative and positive relationships with SST and SSS, respectively, which point to the role of coastal upwelling in driving increases in pDA levels. However, there is some field evidence that DA events may occur at the end stage or transitional period between upwelling and relaxation states (Kudela et al., 2004a,b) when SST and SSS values would still bear

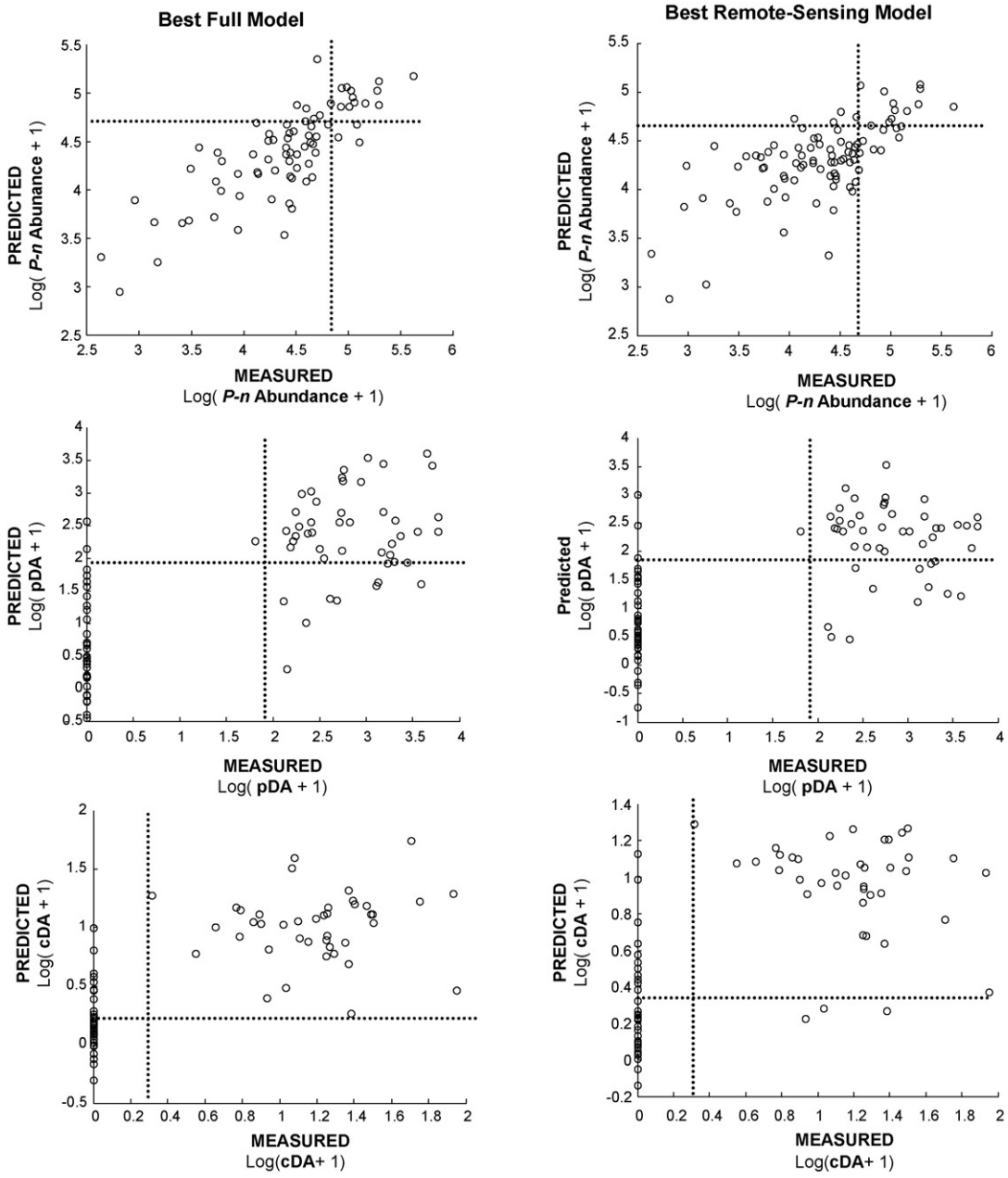

Fig. 7. Results of the best-fit full and remote-sensing models. The dashed lines represent the critical thresholds (5×10^4 cells L^{-1}, 64 ng L^{-1}, and 1.1 pg $cell^{-1}$ for *P-n* abundance, pDA, and cDA, respectively) used to evaluate correct and incorrect model estimates of 'bloom' and/or toxic events.

an upwelling signature but surface nutrient availability would be much diminished from that during early upwelling. Perhaps the lack of importance for CHL in this model, despite its significant correlation with pDA (Table 1), reflects a patchy nature in the biomass field during the end stage of a bloom period when pDA levels would be potentially greatest.

For cDA concentrations, the best full model has a skill of 58% and contains similar predictors to the pDA full model: SST, $a_g(412)$,

Table 3
Model statistics for the three response variables represented as best-fit full models, which include all possible parameters, and the best-fit remote-sensing models, which only employ parameters that can be measured by satellite or other remote utilities.

Variable	Best full model			Best remote-sensing model		
	Coefficients	S_T	N	Coefficients	S_T	N
log(*P-n* Abundance + 1	8.48 − 0 51 [R_{rs}(412/555)] − 0.05 [log(Si:N)] − 83.5 [R_{rs}(555)] − 5.07 [a_p(490)] − 2.28 [R_{rs}(510/555)]	0.75	75	9.2 − 1.40 [R_{rs}(412/555)] − 548.63 [R_{rs} (555)] + 318.16 [R_{rs}(510)] − 0.072 [CHL] − 2.14 [R_{rs}(510/555)]	0.63	89
log(pDA + 1)	−77.2 − 2.42 [R_{rs}(510/555)] − 0.02 [Si:P] − 0.12 [SST] + 2.50 [SSS]	0.58	80	11.37 − 5.79 [R_{rs}(510/555)] − 0.31 [SST] + 1.58 [R_{rs}(490/555)] + 0.003 [rsDOY] − 0.174 [CHL]	0.47	86
log(cDA + 1)	3.5 − 0.15 [SST] + 6.28 [a_g(412)] + 0.02 [SSS] − 1.27 [R_{rs} (510/555)] − 5.06 [a_p(510)]	0.58	75	4.83 − 0.16 [SST] − 48.72 [R_{rs}(412)] − 0.07 [CHL] − 1.21 [R_{rs}(510/555)] − 9.03 [R_{rs}(510)rs]	0.46	72

SSS, R_{rs} (510/555), and $a_p(510)$ (Table 3). With a critical threshold of 1.1 pg DA cell^{-1} (or ~0.32 on the log-transformed scale), the full model correctly predicts almost all (98%) of the bloom observations (Fig. 7). However, it predicts only ~70% of non-bloom observations with ~29% false positive predictions. The most significant association in the model is a negative relationship between cDA levels and SST, again suggestive of the link between cold, upwelled waters and toxin concentration and further supported by the importance of positive SSS in explaining cDA (Table 3). Like the *P-n* abundance full model, the several optical properties in the model for cDA again indicate the presence of either cDOM or other UV-absorbing compounds ($a_g(412)$) and the relationship of absorption/reflectance at 510 and 555 nm with chlorophyll biomass in temperate waters (O'Reilly et al., 1998). The key differences between the pDA and cDA hindcastors are the lack of a macronutrient predictor for cDA concentration and the importance of absorption at 412 nm in explaining the variance of the cellular DA pool.

3.2.4. Remote-sensing models

The models in this section contain components that can all be derived remotely, and given this constraint, they do not perform as well as the full models but may still serve as a useful management tool. The best remote-sensing model for *P-n* abundance was achieved by a similar stepwise process to that used above for the full models, whereby with each addition of *M* variables, only the remotely sensible variables were considered when assessing the true skill. The resulting remote-sensing model contains the predictors R_{rs} (412/555), R_{rs} (555), R_{rs} (510), CHL, and R_{rs} (510/555) (Table 3). With a true skill of 0.63 (cf. $S_T = 0.75$ for the full model), it correctly predicts ~53% of bloom and ~96% of non-bloom observations, with ~4% false positive predictions (Fig. 7). The $R_{rs}(0^+, \lambda)$ and CHL components can all be measured via ocean color imagery, either from the still-operable Sea-viewing Wide-Field-of-View Sensor (SeaWiFS) or the more recent Moderate Resolution Imaging Spectroradiometer (MODIS) Aqua satellites. A second best remote-sensing model was developed by removing the nutrient component from the best full model for *P-n* abundance and substituting the $a_p(490)$ component with R_{rs} (490). Since changes in backscatter are inversely related to changes in absorption, it is reasonable to substitute the $R_{rs}(\lambda)$ value and recalculate the parameter coefficients. This new model performs with slightly less skill ($S_T = 0.61$) and performance in the cost function terms (~50% correct bloom).

The best remote-sensing model for pDA was also achieved by the stepwise process used for the remote-sensing model of *P-n* abundance, whereby only remotely sensible variables were considered at each iterative increase of *M* inputs. The resulting model performs with less skill ($S_T = 0.47$, $N = 86$) than the full model and contains the variables R_{rs} (510/555), SST, R_{rs} (490/555), DOY, and CHL (Table 3, Fig. 7). It correctly predicts ~76% of bloom and ~92% of non-bloom observations, and essentially the same number of false positives (~8%; $n = 3$) as the full model. The reflectance components relate to the presence of chlorophyll absorption at those wavebands and can be estimated from satellite radiometry; the CHL component can be estimated with ocean color algorithms. Advanced Very High Resolution Radiometer (AVHRR) or MODIS satellite imagery allows for the remote estimation of SST values.

The remote-sensing model developed using the stepwise approach described above for pDA, where only the most predictive, remotely sensible variables are retained at each step, yielded less skill than a remote-sensing model created by modifying the best full model for cDA. In other words, when the absorption parameters $a_g(412)$ and $a_p(510)$ in the full cDA model were replaced by their associated $R_{rs}(0^+, \lambda)$ values and the salinity term was replaced by CHL, the hindcastor was then converted to a remote-sensing model with a better true skill ($S_T = 0.48$) than the remote-sensing model developed through the alternative stepwise regression process (Table 3). This best remote-sensing model correctly predicts 95% of bloom and 62% of non-bloom observations with considerably more false positives (38%) than the previous models for pDA and *P-n* abundance (Fig. 7). All components of this model can be estimated with a combination of SeaWiFS, MODIS, and AVHRR satellite imagery.

4. Model validation

An independent dataset of *P-n* abundance and DA concentrations was used to validate the best-fit full and remote-sensing models for the three log-transformed response variables. A full suite of surface physical, chemical, phytoplankton, and domoic acid data were recorded during a toxigenic *P. australis* bloom from 15 to 21 May 2003 on a channel-wide cruise conducted by the SBC-LTER (Anderson et al., 2006). Due to the fact that in situ optical data were not routinely collected on SBC-LTER cruises, for those models which included either absorption or remote-sensing reflectance components, the $R_{rs}(0^+, \lambda)$ retrievals from concurrent SeaWiFS satellite observations for the SBC were substituted. The remote-sensing models were validated with a combination of in situ data for SST values and SeaWiFS data for chlorophyll and $R_{rs}(0^+, \lambda)$ values.

SeaWiFS images for the SBC were obtained from high resolution picture transmission (HRPT) data (Distributed Active Archive Data, Code 902, NASA) and processed using operational algorithms (McClain et al., 2004; Otero and Siegel, 2004). All SeaWiFS overpasses that occurred during the May 2003 cruise period were sampled, resulting in 33 LTER sampling locations with cloud-free retrievals. Of these, the retrievals which most closely matched the shipboard sampling date for a given SBC-LTER station were selected, and a total of 16 locations sampled between 17 and 21 May 2003 were suitable for use in model validation (see Fig. 1). For each of these 16 locations, above water, remote-sensing reflectance was calculated at the six SeaWiFS wavebands (412, 443, 490, 510, 555, and 665 nm; e.g. Westberry and Siegel, 2005).

In order to test the full model for *P-n* abundance using SBC-LTER data, the variable $a_p(490)$ was replaced with R_{rs} (490), which reduces hindcastor performance somewhat ($S_T = 0.67$; 65% correct bloom predictions). Using field values of Si:N and SeaWiFS $R_{rs}(0^+, \lambda)$ data, the measured and predicted values of transformed *P-n* abundance ($N = 15$) from the 2003 event are related by an $r^2 = 0.42$ ($p < 0.01$), and the model correctly predicted 80% of bloom observations (Fig. 8). The remaining predictions were all classified as false negatives ($n = 3$) since none of the measured values of cell abundance from the 2003 bloom fell below the designated bloom threshold of 5.0×10^4 cells L^{-1}. Validation of the best remote-sensing model for *P-n* abundance required only the input of SeaWiFS $R_{rs}(0^+, \lambda)$ values for each component. The remote-sensing model resulted in the same predictions as the full model with 80% of the 2003 bloom measurements correctly identified and 20% false negative predictions ($r^2 = 0.32$, $p = 0.01$; Fig. 8).

Validation of the pDA full model required a combination of SBC-LTER cruise data and SeaWiFS R_{rs} (510/555). The relationship between measured and predicted toxin concentrations for the 2003 bloom ($N = 15$) was the same as for *P-n* abundance ($r^2 = 0.42$, $p < 0.01$). However, the pDA full model correctly predicted 100% of sample values above the critical threshold of 64 ng L^{-1}. Only one of the 15 measured DA values used in the validation test fell below the designated threshold, and this sample was overestimated (i.e. false positive) by ~550 ng L^{-1} by the full model (Fig. 8). The

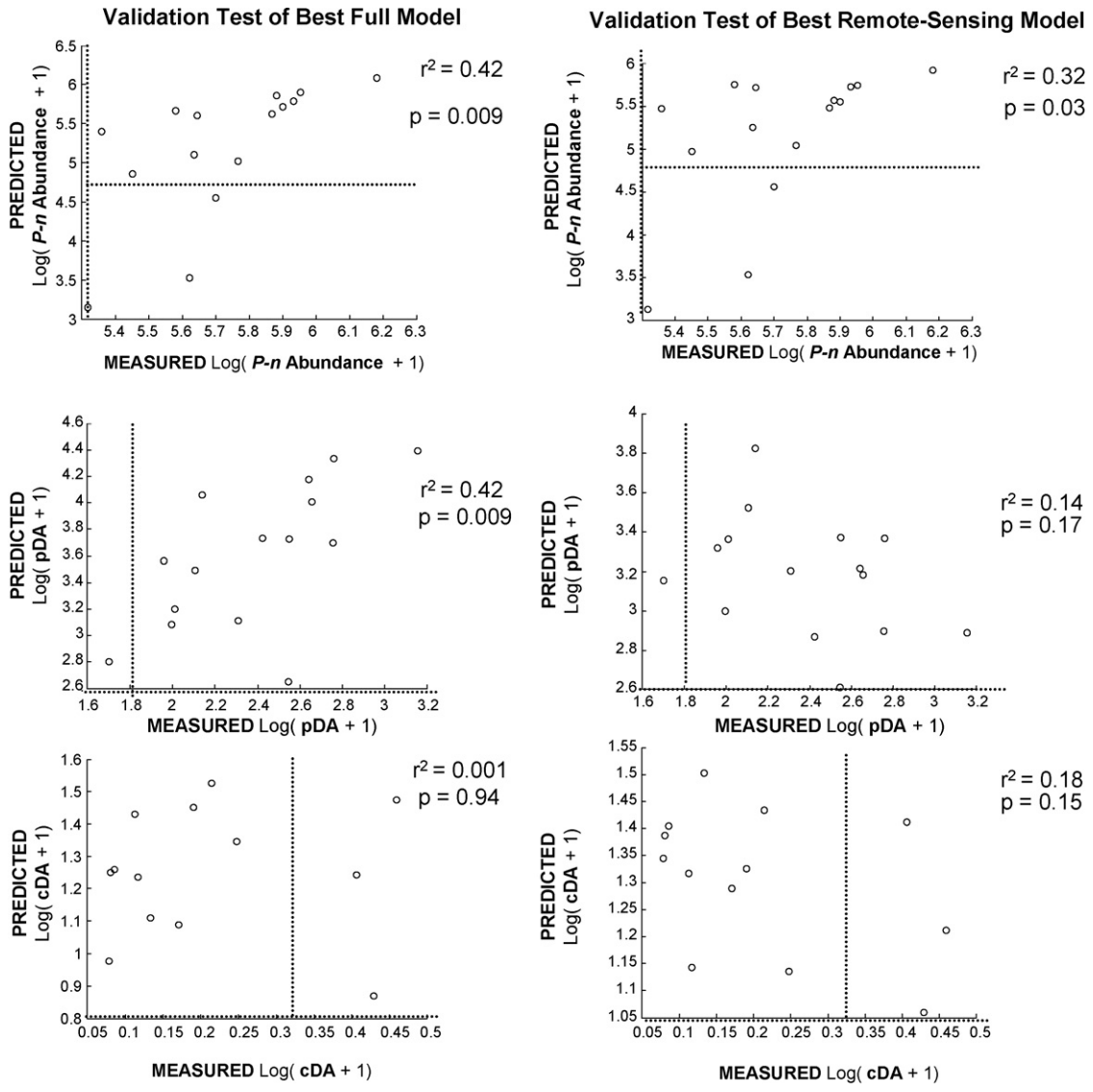

Fig. 8. Using a combination of in situ data and channel-wide $R_{rs}(0^+, \lambda)$ retrievals from a toxigenic *Pseudo-nitzschia australis* bloom independently sampled during an SBC-LTER cruise from 15 to 21 May 2003, the full and remote-sensing models for *P-n* abundance, pDA, and cDA were validated. The r^2 and *p*-values (95% C.I.) give a rough estimate of model performance, while the dashed lines indicate the threshold values used to evaluate model performance.

remote-sensing model for pDA performed similarly to the full model in that it made the same proportion of correct bloom and false positive predictions. However, the much weaker relationship between measured and predicted values ($r^2 = 0.14$, $p = 0.17$, $N = 15$) resulted in an even greater overestimation of the false positive point by ~1350 ng L^{-1} (Fig. 8).

In order to test the best full model for cDA concentrations, the $a_g(412)$ and $a_p(510)$ components were replaced with R_{rs} (0^+, λ) values, which reduced the overall skill of the model by 5%. Using the 2003 bloom survey data ($N = 13$), this modified model correctly categorized all three cDA measurements that were above the critical threshold of 1.1 pg $cell^{-1}$ but overestimated the remaining 10 samples (i.e. 100% false positives). The poor fit between measured and predicted values ($r^2 = 0.001$, $p = 0.94$) is evident in Fig. 8. Validation of the best remote-sensing model using a combination of SeaWiFS $R_{rs}(0^+, \lambda)$ and CHL retrievals with field SST data gave the same results as those for the full model, but with a strong negative relationship between measured and predicted values ($r^2 = 0.18$, Fig. 8). Some of the error in the performance of the remote-sensing model we attribute to error in the SeaWiFS CHL estimates (Otero and Siegel, 2004). However, substitution of in situ fluorometric CHL values for the satellite values actually led to a strong negative relationship between predicted and measured values ($r^2 = 0.52$) and a slightly poorer performance in the cost function terms (i.e. 33% correct bloom observations and 90% false positives).

5. Discussion

The results from this unique time series of environmental and HAB-specific data across a channel-wide transect in the SBC provide a clearer picture of the seasonal and interannual pattern of *Pseudo-nitzschia* spp. blooms in the region than that obtained from previous event-scale studies. These data reveal a new upper limit of cellular and particulate DA values (cDA: 88 pg $cell^{-1}$; pDA: 6000 ng L^{-1}) that exceed earlier field measurements within the SBC (max. cDA ~ 2 pg $cell^{-1}$; max. pDA ~ 1684 ng L^{-1}). Newly reported measurements of DA in the Los Angeles Harbor (Schnetzer et al., 2007) just south of the SCB are currently the highest on record with a maximum cDA of 117 pg $cell^{-1}$ and pDA of

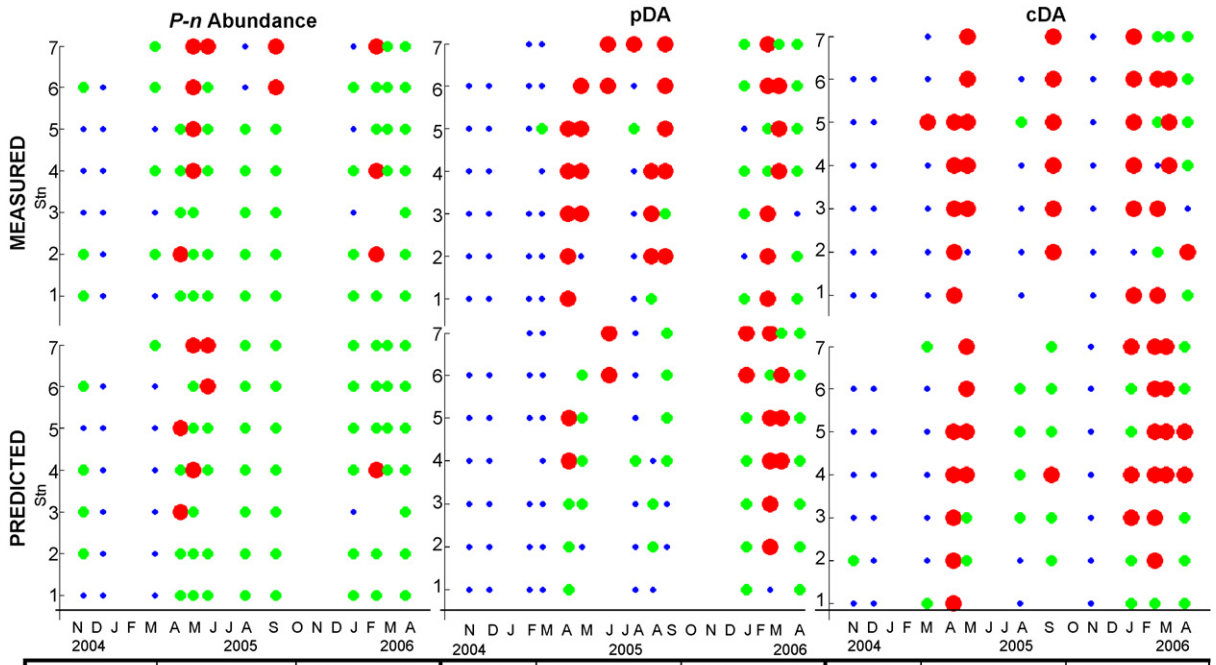

P-n Abundance	Cell Range (cells L^{-1})	% Correctly Predicted	pDA Levels	Conc. Range (ng L^{-1})	% Correctly Predicted	cDA Levels	Conc. Range (pg $cell^{-1}$)	% Correctly Predicted
Low	$0 – 10^4$	65	Low	0 - 64	88	Low	0 - 1	70
Med	10^4 - 10^5	85	Med	64 - 500	56	Med	1 - 10	44
High	$>10^5$	36	High	>500	37	High	>10	54

Fig. 9. Model performance cast as a function of range criteria that assign low, medium, and high levels of *P-n* abundance, pDA, and cDA. For any month in the sampling period, model predictions of cell abundance and toxin levels are compared with observations at each station in the PnB transect, revealing the difficulty in predicting the high end of the range in these parameters.

$\sim$12,000 ng L^{-1}). This may either signify an increase in the magnitude of toxic events over time or a past under-sampling of the spatial and temporal variability of DA concentrations. If the magnitude is indeed increasing, defining the factors responsible still proves elusive. For instance, both 2005 and 2006 were years with toxic blooms and DA-related marine mammal strandings in the SBC. However, the magnitude of the 2005 spring bloom in terms of toxic cell load was twofold greater than that in 2006 (Figs. 2 and 4). Moreover, it is not clear from the mean SST, CHL, or nutrient fields that 2005 was marked by stronger upwelling or other possible driving factors. The reverse, i.e. weaker upwelling, could even be more likely given that the minimum SST and maximum nutrient concentrations in the time series were recorded for March 2006, not 2005. This scenario would seem to support the existing field and laboratory evidence linking nutrient-limitation or overall physiological stress to the magnitude of DA production by *Pseudo-nitzschia* spp., but only with future research could we adequately argue for an association between upwelling and the magnitude of DA events.

6. Model performance

The statistical models developed in this study for estimating the probability of toxigenic *Pseudo-nitzschia* spp. blooms from environmental properties showed much better predictive skill and performance for cell abundance alone than for DA concentrations, whether particulate or cellular (Table 3, Fig. 7). The factors leading to major DA events are often not the same conditions favorable to *Pseudo-nitzschia* spp. bloom development, nor were these factors necessarily measured as part of our sampling effort. In the case of cell abundance, values were best estimated by a suite of chlorophyll-related optical parameters and the ratio of $Si(OH)_4$ to NO_3^-. Together, these factors seem to identify the build-up of biomass and the uptake of silicic acid by diatoms. Values of both pDA and cDA were best estimated by upwelling and biomass-associated relationships with R_{rs} (510/555), SST, and SSS. The key difference between the two toxin models is the low Si:P requirement for estimates of pDA and the cDOM absorption parameter for estimates of cDA. This suggests that environmental variability in cellular DA concentration is more associated with growth stage of the *Pseudo-nitzschia* spp. population while variations in the particulate DA pool are more controlled by ambient nutrient availability.

When assessed using a single, bloom-threshold value, the models exhibit a maximum 58% skill at accurately estimating toxin concentration from in situ or remotely sensed data and a maximum 98% probability for bloom-level DA loads. An additional method for judging model performance is shown in Fig. 9. The single thresholds are further subdivided to determine probabilities of low, medium, and high toxic bloom levels, which is useful from an operational perspective (e.g. C. Brown, http://coastwatch.noaa.gov/cbay_hab). We use the threshold values $\sim 10^4$ cells L^{-1}, 64 ng L^{-1}, and $\sim$1 pg $cell^{-1}$ for *P-n* abundance, pDA, and cDA, respectively, to distinguish low from medium bloom/toxin levels. The threshold values for high levels (10^5 cells L^{-1}, 500 ng L^{-1}, 10 pg $cell^{-1}$) were chosen to roughly reflect conditions associated with

extreme DA/mammal stranding events in CA (Fig. 9, Trainer et al., 2000; Anderson et al., 2006; Schnetzer et al., 2007). While it is encouraging that the models differentiate low bloom/toxin levels from all others with reasonable accuracy (max. 88%), the models are less accurate at differentiating medium and high toxic bloom levels at a given station during a given month (Fig. 9). This underscores the challenge ahead for predicting extreme DA events in the environment.

When all models were applied to the independent *Pseudo-nitzschia australis* bloom dataset from May 2003, they greatly over-predicted DA concentration, both particulate and cellular (Fig. 8). One important, external source of error to consider in the validation of these models is the poor statistical match-up between SeaWiFS R_{rs} (0^+, λ) retrievals from May 2003 and those reflectance spectra used in model development which were acquired from shipboard radiometer data. Until regional atmospheric correction algorithms are better tuned, this may remain a hurdle for detection models that incorporate remote-sensing reflectance components from SeaWiFS or MODIS-Aqua. Several other possible sources of error in the HAB models are considered below.

7. Circulation effects

The interaction between regional circulation and surface phytoplankton biomass may help explain the difficulty in accurately predicting local *Pseudo-nitzschia* spp. abundance and DA levels from the environmental properties used in this modeling exercise. For example, Marchetti et al. (2004) found that eddy circulation and horizontal advection along the Washington coast are important determinants of DA accumulation. In the SBC, seasonal mesoscale eddies also appear to influence the entrainment of toxigenic cells and subsequent accumulation of high cDA levels within convergent eddy boundaries (Anderson et al., 2006). In both cases, toxic cells were shown to have accumulated at convergent fronts most likely according to the mechanism described by Franks (1992) for non-motile phytoplankton forms at frontal zones. This type of physically induced accumulation of HABs has important implications for the spatial prediction of toxicity, which may require additional knowledge of the flow field as can now be achieved using HF radar determinations of surface currents.

To better understand possible circulation effects on predictions of local toxin concentration in this study, we focused on the large overestimation of cDA concentration in samples where none was detected. These false positive populations from both the full and remote-sensing models for cDA were examined in terms of what distinguishes them from the correct estimates of cDA. In the case of the full cDA model, a discrimination analysis using a Students *t*-test with 95% confidence limits shows that the correct estimates of cDA above the 1.1 pg cell^{-1} threshold were samples that co-occurred with significantly lower SST, higher CHL and nutrient concentrations, lower R_{rs} (412) and R_{rs} (510/555), and higher $a_p(\lambda)$ values than the samples in the false positive population. This is generally due to the fact that the majority of high cDA samples are from spring cruises (Fig. 2) when seasonal upwelling would lead to cold, nutrient-rich, high-biomass (i.e. high particulate absorption, low remote-sensing reflectance) surface conditions. The one exception was the high cDA event (9–88 pg cell^{-1}) recorded on September 9, 2005 (Fig. 3) which was concurrent with moderate to bloom-level *Pseudo-nitzschia* abundances (2.9×10^4–1.1×10^5 cells L^{-1}) and typified by warm SST, low CHL and nutrient concentrations, and higher R_{rs} (0^+, λ) values relative to the spring bloom samples. Interestingly, this summer-time DA event appears from MODIS-Aqua CHL imagery throughout September 2005 to have been initiated by favorable conditions north of or just at Pt. Conception and then advected into the SBC where surface waters were then entrained into what might be a cyclonic eddy (Fig. 10a). In other words, conditions *within* the SBC were quite possibly not responsible for initiating the toxic bloom in this instance. However,

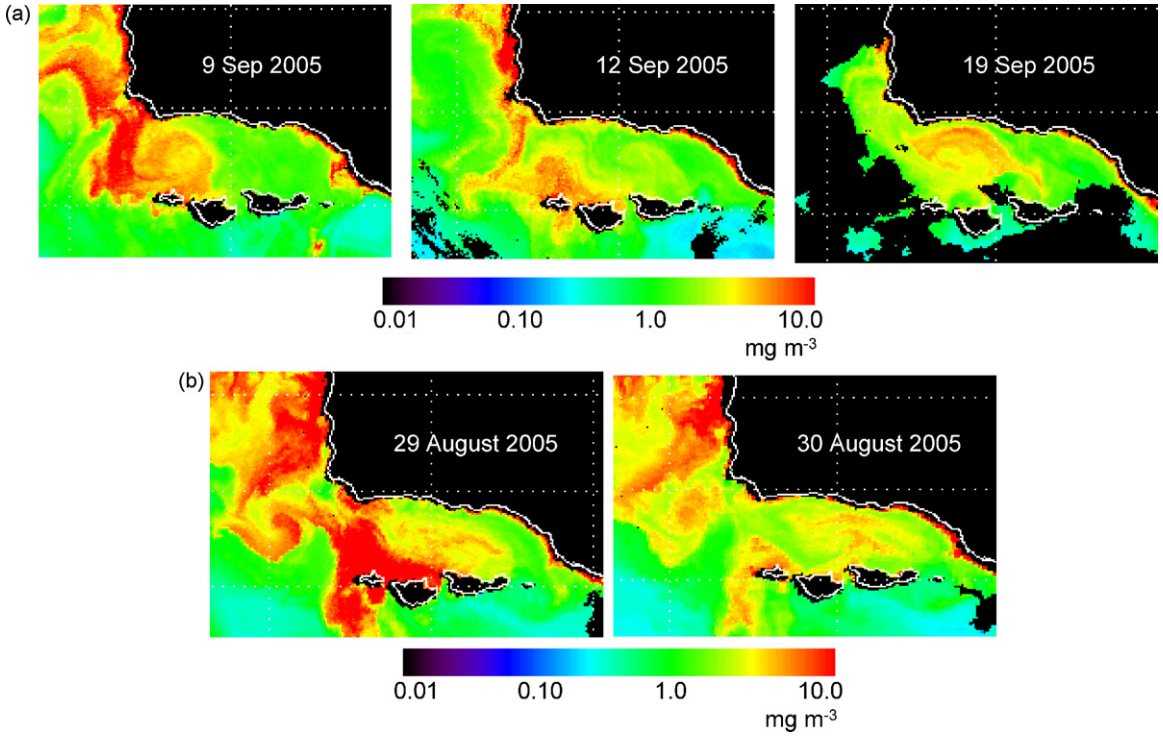

Fig. 10. MODIS-Aqua chlorophyll imagery from (a) September and (b) August 2005 indicates advection of high-biomass waters from Pt. Conception into the western SBC, which may be the source of the high cDA event recorded on 20 September 2005 and high pDA event on 30 August 2005.

secondary circulation effects within the SBC may have further retained cells in nutrient-poor surface waters conducive to increased toxicity (Pan et al., 1998).

The result of this circulation effect is that inclusion of the September 2005 bloom samples in the training dataset forced the *Pseudo-nitzschia* abundance and DA concentration models with properties potentially unrelated to local, within-channel, toxic bloom production. Indeed, the discriminant analysis reveals that properties concurrent with samples in the false positive population for the cDA full model are indistinguishable from those during the September 2005 bloom. This becomes particularly important for the remote-sensing model of cDA which is based on SST, CHL, R_{rs} (412), and R_{rs} (510/555), all of which are significantly different for the September 2005 population than for the remaining correct bloom estimates. Similarly, the false positive population from the full model of *Pseudo-nitzschia* abundance shares the same traits as samples of *Pseudo-nitzschia* abundance from the September 2005 bloom and is significantly different from the correct bloom estimates with respect to CHL, R_{rs} (443), and a_p(412). It therefore appears that the summertime anomaly of 2005 forced the *Pseudo-nitzschia* abundance model in the same way it did the cDA models but to a lesser extent in terms of the percentage of false positives (~6% vs. ~29%, respectively).

While the false positives signify those predictions of high toxin concentration where no toxin existed, the false negative population represents those samples where toxin concentrations were above the designated threshold but were estimated below it. From a management perspective, these scenarios could be considered more worrisome (e.g. Wekell et al., 2002) and for predictions of pDA, the models produced more false negative (~20%) results than false positive (~9%). Discrimination of this population with respect to the correct toxin estimates reveals that the underestimates occurred during times of significantly higher SST, lower SSS, lower CHL and nutrient concentrations, and higher R_{rs} (0^+, λ) values. In short, ~75% of the false negatives are from summertime episodes of increased pDA in August–September 2005. It is clear that DA events in summer pose the greatest predictive problems. MODIS-Aqua CHL images again offer a secondary filter through which to assess the increased probability of toxic blooms during summer months (Fig. 10b). Validated imagery prior to and during the 30 August 2005 cruise shows a similar scenario to that later in September with advection of waters from Pt. Conception into the western Channel (Fig. 10b). Because conditions along the coast north of the SBC are more conducive to bloom development during summer than they are within the SBC, these scenarios require closer examination when using remote detection methods for HABs and may indicate the need for season-specific models.

8. Macronutrient control

Along with the possibility of trace metal control not measured as part of this study (Maldonado et al., 2002; Ladizinsky, 2003; Wells et al., 2005), many laboratory and field studies have demonstrated the association between Si-limitation and DA production when $Si(OH)_4$ concentrations are low (Pan et al., 1996, 1998; Kudela et al., 2004a,b; Marchetti et al., 2004), though the exact mechanism is not clear. We can assess the potential role of Si-limitation as expressed through Si:N or Si:P ratios when Si concentrations are at limiting levels. The latter appears as a significant predictor in the full models of *Pseudo-nitzschia* abundance and pDA. For the full pDA model presented in Table 3, there is a negative relationship with Si:P, suggesting a correlation with Si-limitation. For the *Pseudo-nitzschia* abundance model, on the other hand, a negative relationship with Si:N would also indicate an association with Si-limitation but when NO_3^- concentrations are more replete (Table 3). This is in contrast to field evidence from Monterey Bay (Kudela et al., 2004a,b), Southern California (Schnetzer et al., 2007), and the SBC (Anderson et al., 2006) which did not reveal a significant link between the *Pseudo-nitzschia*-specific biomass and Si-limitation (Kudela et al., 2004a,b) nor Si:N and Si:P ratios (Anderson et al., 2006) despite significant relationships for DA production. However, disproportionate drawdown of $Si(OH)_4$ is expected for *Pseudo-nitzschia* blooms under nutrient-replete conditions when they are capable of maintaining an Si:N of ~2 (Pan et al., 1996) compared with the Si:N ~1 for other diatoms (Brzezinski, 1985; Turner et al., 1998). At the onset of Si-limitation, they can reduce $Si(OH)_4$ uptake (Pan et al., 1996) and potentially out-compete other diatoms (Egge and Aksnes, 1992) during the nutrient-poor transitional stages from upwelling periods to relaxation periods (Kudela et al., 2004a,b).

Interestingly, while Si-limitation might help explain pDA concentrations, the full cDA model does not include any nutrient parameters, which is consistent with findings from the May 2003 bloom in the SBC when only pDA distributions were associated with nutrient concentrations, while cDA was most correlated with variability in the SST field (Anderson et al., 2006). However, in their efforts to predict cellular DA levels in populations of *P. pungens f. multiseries*, Blum et al. (2006) derived statistical models which did rely on nutrient ratio indicators of Si-limitation. The difference there was perhaps their inclusion of a large laboratory dataset of cDA in cultures where Si-limitation is more easily forced and observed. Along with SST, almost all the parameters in our full model for cDA can be remotely sensed with the exception of SSS (though satellite-derived salinity products are forthcoming with the NASA Aquarius mission.). The reduction in skill between the full (S_T = 0.60) and remote-sensing models (S_T = 0.48) for cDA may either be attributed to the replacement of SSS with CHL or by the replacement of the absorption components with R_{rs} (412) and R_{rs} (510). It is also important to note that while the remote-sensing model for cDA has a greater skill than that for pDA, the two pDA models performed better in the cost function terms (Figs. 7 and 8). Ultimately, the development and validation of a remote-sensing model for accurately predicting DA concentrations was more successful for pDA than for cDA, despite the apparently greater dependence of the particulate pool on the in situ nutrient regime.

9. Conclusions

For detection of toxigenic blooms of *Pseudo-nitzschia* in the SBC, models that accurately predict environmental DA concentrations will be more helpful to coastal managers than those that only estimate the abundance of potentially toxic cells of *Pseudo-nitzschia* spp. The empirical method used here to develop a model for remotely detecting the particulate pool of DA in the SBC is useful in that it generally constrains estimates to the presence or absence of pDA but does not accurately estimate absolute concentrations of DA. Current methods for safeguarding the public from harmful DA events rely on the monitoring of bivalve mollusc populations with an FDA regulatory limit of 20 ppm (e.g. Lefebvre et al., 2002). However, variations in depuration times and other aspects of invertebrate physiology (e.g. Ferdin et al., 2002) do not allow for the easy translation of this value to an in situ DA concentration for which no regulatory limit presently exists. Furthermore, the relationship between environmental DA levels and neurotoxicity in fish and mammals remains elusive (Lefebvre et al., 2002). Remote detection tools for DA presence/absence can however be used by managers to track the fate and transport of toxin-containing, hydrographic features through the use of near real-time satellite imagery of ocean color, SST, and surface currents which may further guide the selective testing of molluscs in high-

risk locations along the SBC coast. Future efforts will employ a combination of toxin-monitoring, satellite, and dynamically downscaled forecasting products to test these empirical models in the Santa Barbara Channel. This approach may also prove useful for the entire Southern California Bight region where large DA events appear to be a recent phenomenon (Busse et al., 2006; Schnetzer et al., 2007) with the potential to increase in intensity in the years to come.

Acknowledgements

This study was supported by NASA, NOAA, Channel Islands National Marine Sanctuary, and NSF support of the Plumes and Blooms (NAS5-00201) and Santa Barbara Coastal LTER projects (OCE 9982105). Funding was also provided by a UC Toxic Substances Research and Training Program (UC TSR&TP) travel grant and a NASA Earth System Science Graduate Fellowship for C. Anderson (06-ESSF-06R-12). We thank N. Guillocheau, D. Court, D. Menzies, T. Kostadinov, and the crew of the R/V *Shearwater* for assistance with data collection each month. Special thanks go to A. Alldredge for providing her inverted microscope, to A. Roberts and M. Armstrong for help with HPLC analysis of toxin samples, and to Erik Fields for satellite retrievals and imagery.[SS]

References

Anderson, C.R., Brzezinski, M.A., Washburn, L., Kudela, R., 2006. Circulation and environmental conditions during a toxigenic Pseudo-nitzschia australis bloom in the Santa Barbara Channel, California. Marine Ecology Progress Series 327, 119–133.

Bates, S.S., Garrison, D.L., Horner, R.A., 1998. Bloom dynamics and physiology of domoic-acid-producing Pseudo-nitzschia species. In: Anderson, D.M., Cembella, A.D., Hallegraeff, G.M. (Eds.), Physiological Ecology of Harmful Algal Blooms. Springer-Verlag, Heidelberg, pp. 267–292.

Blum, I., Subba Rao, D.V., Pan, Y., Swaminathan, S., Adams, N.G., 2006. Development of statistical models for prediction of the neurotoxin domoic acid levels in the pennate diatom Pseudo-nitzschia pungens f. multiseries utilizing data from cultures and natural blooms. In: Rao, D.V.S. (Ed.), Algal Cultures: Analogues of Blooms and Applications, vol. 2. Science Publishers, Enfield, NH, pp. 891–930.

Brown, C.W., Yoder, J.A., 1994. Coccolithophorid blooms in the global ocean. Journal of Geophysical Research 99, 7467–7482.

Brzezinski, M.A., 1985. The Si:C:N ratio of marine diatoms: interspecific variability and the effect of some environmental variables. Journal of Phycology 21, 347–357.

Busse, L.B., Venrick, E.L., Antrobus, R., Miller, P.E., Vigilant, V., Silver, M.W., Mengelt, C., Mydlarz, L., Prezelin, B., 2006. Domoic acid in phytoplankton and fish in San Diego, CA, USA. Harmful Algae 5, 91–101.

Campbell, J.W., 1995. The lognormal distribution as a model for bio-optical variability in the sea. Journal of Geophysical Research 100 (13), 213–237 254.

Craig, S.E., Lohrenz, S.E., Lee, Z., Mahoney, K.L., Kirkpatrick, G.J., Schofield, O.M., Steward, R.J., 2006. Use of hyperspectral remote sensing reflectance for detection and assessment of the harmful alga, Karenia brevis. Applied Optics 45 .

Davis, R.E., 1976. Predictability of sea surface temperature and sea level pressure anomalies over the North Pacific Ocean. Journal of Physical Oceanography 6, 249–266.

Davis, R.E., 1978. Predictability of sea level pressure anomalies over the North Pacific Ocean. Journal of Physical Oceanography 8 .

Egge, J.K., Aksnes, D.L., 1992. Silicate as regulating nutrient in phytoplankton competition. Marine Ecology Progress Series 83, 281–289.

Emery, W.J., Thomson, R.E., 1997. Data Analysis Methods in Physical Oceanography. Elsevier Science Inc, Pergamon, New York.

Ferdin, M.E., Kvitek, R.G., Bretz, C.K., Powell, C.L., Doucette, G.J., Lefebvre, K.A., Coale, S., Silver, M.W., 2002. Emerita analoga (Stimpson)—possible new indicator species for the phycotoxin domoic acid in California coastal waters. Toxicon 40, 1259–1265.

Franks, P.J.S., 1992. Sink or swim: accumulation of biomass at fronts. Marine Ecology Progress Series 82 .

Fritz, L., Qulliam, M.A., Wright, J.L.C., Beale, A.M., Work, T.M., 1992. An outbreak of domoic acid poisoning attributed to the pennate diatom Pseudonitzschia australis. Journal of Phycology 28, 439–442.

Fryxell, G.A., Villac, M.C., Shapiro, L.P., 1997. The occurrence of the toxic diatom genus Pseudo-nitzschia (Bacillariophyceae) on the West Coast of the USA, 1920–1996: a review. Phycologia 36, 419–437.

Harms, S., Winant, C.D., 1998. Characteristic patterns of the circulation in the Santa Barbara Channel. Journal of Geophysical Research 103, 3041–3065.

Hasle, G.R., 1978. The inverted-microscope method. In: Sournia, A. (Ed.), Phytoplankton Manual. UNESCO, Paris, pp. 88–96.

Iglesias-Rodriguez, M.D., Brown, C.W., Doney, S.C., Kleypas, J., Kolber, D., Kolber, Z., Hayes, P.K., Falkowski, P.G., 2002. Representing key phytoplankton functional groups in ocean carbon cycle models; coccolithophorids. Global Biogeochemical Cycles 16, 20.

Johnson, K.S., Petty, R.L., Thompsen, J., 1985. Flow injection analysis for seawater macronutrients. In: Zirino, A. (Ed.), Mapping Strategies in Chemical Oceanography, vol. 209. pp. 7–30.

Kahru, M., Mitchell, B.G., 1998. Spectral reflectance and absorption of a massive red tide off southern California. Journal of Geophysical Research 103 (21), 601–621 609.

Knap, A.H., Michaels, A.F., Dow, R.L., Johnson, R.J., Gundersen, K., Sorensen, J.C., Close, A.R., Howse, F., Hammer, M., Bates, N., Doyle, A., Waterhouse, T., 1993. BATS Methods Manual, vol. version 3. U.S. JGOFS Planning Office, Woods Hole.

Kudela, R., Cochlan, W., Roberts, A., 2004a. Spatial and temporal patterns of Pseudo-nitzschia spp. in central California related regional oceanography. In: Steidenger, K.A., Landsberg, J.H., Tomas, C.R., Vargo, G.A. (Eds.), Harmful Algae 2002. Florida and Wildlife Conservation Commission, Florida Institute of Oceanography, and Intergovernmental Oceanographic Commission of UNESCO.

Kudela, R., Pitcher, G., Probyn, T., Figueiras, F., Moita, T., Trainer, V.L., 2005. Harmful algal blooms in coastal upwelling systems. Oceanography 18, 185–197.

Kudela, R., Roberts, A., Armstrong, M., 2004b. Laboratory analyses of nutrient stress and toxin production in Pseudo-nitzschia spp. from Monterey Bay, California. In: Steidenger, K.A., Landsberg, J.H., Tomas, C.R., Vargo, G.A. (Eds.), Harmful Algae 2002. Florida and Wildlife Conservation Commission, Florida Institute of Oceanography, and Intergovernmental Oceanographic Commission of UNESCO.

Ladizinsky, N., 2003. The Influence of Dissolved Copper on the Production of Domoic Acid by Pseudo-Nitzschia species in Monterey Bay, California Laboratory Experiments and Field Observations. California State University, Monterey Bay.

Lefebvre, K.A., Bargu, S., Kieckhefer, T., Sliver, M.W., 2002. From sanddabs to blue whales: the pervasiveness of domoic acid. Toxicon 40, 971–977.

Maldonado, M.T., Hughes, M.P., Rue, E.L., Wells, M.C., 2002. The effect of Fe and Cu on growth and domoic acid production by Pseudo-nitzschia multiseries and Pseudo-nitzschia australis. Limnology and Oceanography 47, 515–526.

Marchetti, A., Trainer, V.L., Harrison, P.J., 2004. Environmental conditions and phytoplankton dynamics associated with Pseudo-nitzschia abundance and domoic acid in the Juan de Fuca eddy. Marine Ecology Progress Series 281, 1–12.

McClain, C.R., Feldman, G.C., Hooker, S.B., 2004. An overview of the SeaWiFS project and strategies for producing a climate research quality global ocean bio-optical time series. In: Siegel, D.A., Thomas, A.C., Marra, J. (Eds.), Views of Ocean Processes from the Sea-viewing Wide Field-of-view Sensor (SeaWiFS) Mission, vol. 2, 51. Pergamon-Elsevier Science, Ltd, Oxford, England, pp. 5–42.

McPhee-Shaw, E.E., Siegel, D.A., Washburn, L., Brzezinski, M.A., Jones, J.L., Leydecker, A., Melack, J., 2007. Mechanisms for nutrient delivery to the inner shelf: observations from the Santa Barbara Channel. Limnology and Oceanography 52 (5), 1748–1766.

Mengelt, C., 2006. How two species of the diatom genus Pseudo-nitzschia respond to 18 adverse conditions: P. australis and P. multiseries UV-photoecology, darksurvival, 19 and seasonal abundance at two coastal sites in Central California. Ph.D. Thesis. 20 University of California, Santa Barbara.

Mueller, J.L., Austin, R.W., 1995. Ocean optics protocols for SeaWiFS validation. In: Hooker, S.B., Firestone, E.R., Acker, J.G. (Eds.), NASA Technical Memo, vol. 25. NASA Goddard Space Flight Center, Greenbelt, MD, pp. 67.

O'Reilly, J.E., Maritorena, S., Mitchell, B.G., Siegel, D.A., Carder, K.L., Garver, S.A., Kahru, M., McClain, C., 1998. Ocean color chlorophyll algorithms for SeaWiFS. Journal Of Geophysical Research-Oceans 103, 24937–24953.

Oey, L.-Y., Wang, D.-P., Hayward, T.L., Winant, C.D., Hendershott, M., 2001. Upwelling" and "cyclonic" regimes of the near-surface circulation in the Santa Barbara Channel. Journal of Geophysical Research 106, 9213–9222.

Otero, M.P., Siegel, D.A., 2004. Spatial and temporal characteristics of sediment plumes and phytoplankton blooms in the Santa Barbara Channel. Deep-Sea Research II 51, 1129–1149.

Pan, Y., Bates, S.S., Cembella, A.D., 1998. Environmental stress and domoic acid production by Pseudo-nitzschia: a physiological perspective. Natural Toxins 6, 127–135.

Pan, Y., Subba Rao, D.V., Mann, K.H., Li, W.K.W., Harrison, W.G., 1996. Effects of silicate limitation on production of domoic acid, a neurotoxin, by the diatom Pseudo-nitzschia multiseries. II. Continuous culture studies. Marine Ecology Progress Series 131, 235–243.

Perl, T.M., Bedard, L., Kosatsky, T., Hockin, J.C., Todd, E.C.D., Remis, R.S., 1990. An outbreak of toxic encephalopathy caused by eating mussels contaminated with domoic acid. New England Journal of Medicine 322, 1775–1780.

Pocklington, R., Milley, J.E., Bates, S.S., Bird, C.J., De Freitas, A.S.W., Quilliam, M.A., 1990. Trace determination of domoic acid in seawater and phytoplankton by high-performance liquid chromatogrphy of the fluorenylmethoxycarbonyl (FMOC) derivative. International Journal of Environmental Analytical Chemistry 38, 351–368.

Rue, E.L., Bruland, K.W., 2001. Domoic acid binds iron and copper: a possible role for the toxin produced by the marine diatom Pseudo-nitzschia. Marine Chemistry 76, 127–134.

Sathyendranath, S., Subba Rao, D.V., Chen, Z., Stuart, V., Platt, T., Bugden, G.L., Jones, W., Vass, P., 1997. Aircraft remote sensing of toxic phytoplankton blooms: a case study from Cardigan River, Prince Edward Island. Canadian Journal of Remote Sensing 23, 15–23.

Schnetzer, A., Miller, P.E., Schaffner, R.A., Stauffer, B.A., Jones, B.H., Weisberg, S.B., DiGiacomo, P.M., Berelson, W.M., Caron, D.A., 2007. Blooms of Pseudo-nitzschia and domoic acid in the San Pedro Channel and Los Angeles harbor areas of the Southern California Bight, 2003–2004. Marine Ecology Progress Series 6, 327–387.

Scholin, C.A., Gulland, F., Doucette, G.J., Benson, S., Busman, M., Chavez, F.P., Cordaro, J., DeLong, R., De Vogelaere, A., Harvey, J., Haulena, M., Lefebvre, K.A., Lipscomb, T., Loscutoff, S., Lowenstine, L.J., Marin III, R., Miller, P.E., McLellan, W.A., Moeller, P.D.R., Powell, C.L., Rowles, T., Silvagni, P., Silver, M.W., Spraker, T., Trainer, V.L., Van Dolah, F.M., 2000. Mortality of sea lions along the central California coast linked to a toxic diatom bloom. Nature 403, 80–83.

Siegel, D.A., Dickey, T.D., 1986. Variability of net longwave radiation over the Eastern North Pacific Ocean. Journal of Geophysical Research 91, 7657–7666.

Stumpf, R.P., Culver, M.E., Tester, P.A., Tomlinson, M., Kirkpatrick, G.J., Pederson, B.A., Truby, E., Ransibrahmanakul, V., Soracco, M., 2003. Monitoring Karenia brevis blooms in the Gulf of Mexico using satellite ocean color imagery and other data. Harmful Algae 2, 147–160.

Subramanian, A., Carpenter, E.J., 1994. An empirically derived protocol for the detection of blooms of the marine cyanobacterium Trichodesmium using CZCS imagery. International Journal of Remote Sensing 15, 1559–1569.

Toole, D.A., Siegel, D.A., 2001. Modes and mechanisms of ocean color variability in the Santa Barbara Channel. Journal of Geophysical Research 106 (26), 927–985 000.

Trainer, V.L., Adams, N.G, Bill, B.D., Stehr, C.M., Wekell, J.C., Moeller, P.D.R., Busman, M., Woodruff, D., 2000. Domoic acid production near California coastal upwelling zones, June 1998. Limnology and Oceanography 45, 1818–1833.

Trainer, V.L., Hickey, B.M., Horner, R.A., 2002. Biological and physical dynamics of domoic acid production off the Washington coast. Limnology and Oceanography 47, 1438–1446.

Turner, R.E., Qureshi, N., Rabalais, N.N., Dortch, Q., Justic, D., Shaw, R.F., Cope, J., 1998. Fluctuating silicate:nitrate ratios and coastal plankton food webs. In: Proceedings of the National Academy of Sciences. 95, pp. 13048–13051.

Wekell, J.C., Trainer, V.L., Ayres, D., Simons, D., 2002. A study of spatial variability of domoic acid in razor clams: recommendations for resource management on the Washington coast. Harmful Algae 1, 35–43.

Wells, M.L., Trick, C.Q., Cochlan, W.P., Hughues, M.P., Trainer, V.L., 2005. Domoic acid: the synergy of iron, copper, and the toxicity of diatoms. Limnology and Oceanography 50 (60), 1908–1917.

Westberry, T., Siegel, D.A., 2005. An improved bio-optical model for the remote sensing of Trichodesmium spp. blooms. Journal of Geophysical Research 110.

Winant, C.D., Dever, E.P., Hendershott, M.C., 2003. Characteristic patterns of shelf circulation at the boundary between central and southern California. Journal of Geophysical Research 108, 3021.

Wright, J.L.C., Quilliam, M.A., 1995. Methods for domoic acid, the amnesic shellfish poisons. In: Manual on Harmful Marine Microaglae, vol. 33, Intergovernmental Oceanographic Commission Manuals and Guides for UNESCO, Paris, pp. 113–133.